DCATT Report

DCATT Deep PSF Test

Identification Number: OPTI-ANLS-2
Date: Monday, November 08, 1999
Revision: A
Authors: C. Bowers, D. Redding, S. Basinger, L.Burns, D. Lindler, T. Norton

Introduction:

The purpose of this test was to directly measure the PSF in DCATT following the initial stage of fine phasing. In the current test configuration, the image core will be poorly sampled by the detector and so this test concentrates on a first appraisal of the distribution of light outside the PSF core. In order to reveal faint features of the PSF and not saturate the limited dynamic range of the CCD detector, a number of images were acquired and added together after the test. This series of snapshots, taken over a period of several hours, also allows a longer characterization of system stability than has been previously obtained.

Summary of Results:

1) The PSF has a sharp core (~2 pixels fwhm), surrounded by a roughly square area of very faint light, extending 10-15 pixels from center. Beyond this is a region of brighter, scattered light, about 7 pixels wide, which contains about 7% of the total light in the image. This PSF structure results from the effects of the correcting, deformable mirror (DM) located at a pupil. Low spatial frequencies in the pupil are well corrected by the DM and give rise in the image to the sharp core and adjacent low light level. Beyond the Nyquist frequency of the DM control, residual wavefront error (WFE) results in scattering, far from the sharp core and leads to reduced MTF in the image at low spatial frequencies. Using a simple model of the residual WFE in the DM, the halo scattering should fall approximately as λ^{-2} resulting in a halo containing only ~1% of the total light at 2 microns. Comparison of the experimentally determined deep image with images generated from phase retrieval and pupil imagery show the same general features - a narrow core, a dark approximately square region and surrounding halo. The core in particular is better matched by convolving the projected model to simulate various blurring effects.
2) During a 70 minute period, the image centroids showed a small but systematic motion across the detector amounting to about 0.4 pixels in X(horizontal) and 0.2 pixels in Y(vertical). The source of this drift is not known. The wavefront error monotonically increased after the initial settings from $0.0395\lambda_{633}$ rms to $0.046\lambda_{633}$ rms waves in a period of 8 hours.

Test Details:

The test was conducted on two days, September 28-29, 1999, with the first day used to exercise DM flattening and the second day used to obtain the data used in this analysis. The test configuration included the following components: the source module (SM), the telescope simulator module (TSM), the nominal aft optics components (AO) and the CCD detector and stage comprising the wave front sensor (WFS). The TSM deformable mirror (TSM/DM) was not activated during the test; electronic components for it's operation were being repaired.

The Xinetics DM (AO/DM) was used to flatten the wavefront using an initial flattening file. The standard phase retrieval and control software were used throughout the test series initially to provide the "best" flat by controlling the AO/DM and then to monitor the stability of the wavefront with time.

The SM Xenon source was used for all images (including the focus sequence images) with the 633nm, 3nm width filter in place and the 10%ND filter. To avoid saturation, exposure times were set to 0.16 or 0.17s for all images. A series of 103 images were acquired, which upon co-adding gave a peak pixel value of over 10^6 counts. All images collected consisted of 512x512 pixels. The image series was split into two parts. The initial 23 images were acquired with the CCD camera stage at a setting of 0 mm offset. Following this image set, a focus scan was made with the camera to see if a more precise nominal focus setting should be used. The nominal 0 focus position was found to be a reasonable focus setting (some astigmatism is present - 0 focus appears to be near the best compromise focus). The remaining 80 images were acquired. Dark frames (SM shutter closed) were obtained following each nominal image to account for any stray light as well as to remove the CCD bias. This long series of dark frames would also allow the bias stability and stray light stability in the room to be assessed.

Data Analysis:

1) Focus Sweep

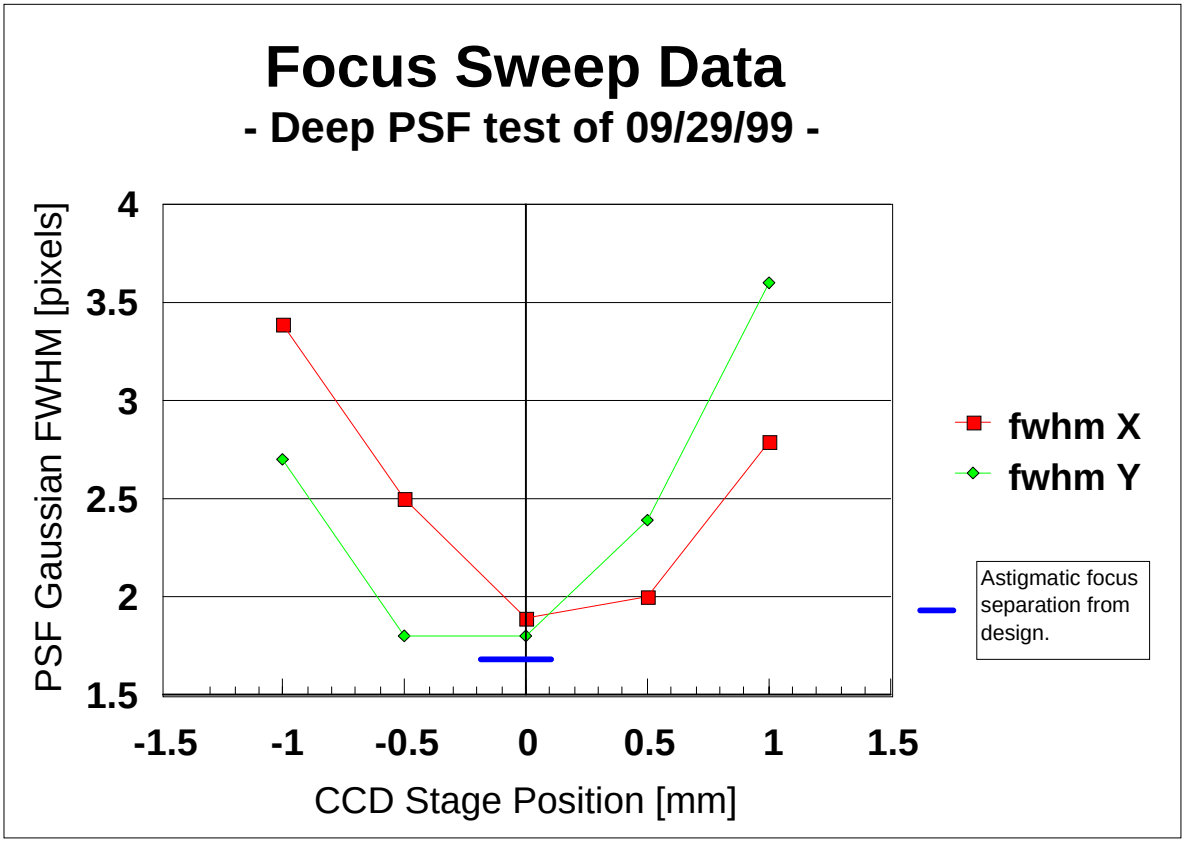

Figure 1: The results of an image focal sweep near the nominal focus (0 position). The image fwhm was determined by Gaussian fitting the 3 pixel wide psf profiles in the horizontal (X) and vertical (Y) directions. The blue, horizontal line represents the separation of the astigmatic foci in the focal plane.

The figure above shows the Gaussian fit fwhm in pixels from 3 pixel wide horizontal and vertical slices (X,Y) from a set of focus sweep images obtained just after deep psf image #23. Fitting was done with the ACSLOOK package fitting routine.

The control system for this test (DM flattening routine) was designed to adjust the DM to match the nominal optical design. That is the wavefront reference surface with respect to which the DM is adjusted, is the wavefront reference surface inherent in the original optical design. Thus the result of perfectly "flattening" the DM is to adjust the wavefront to match that expected in the design, and contains the same aberrations as in that design. The current optical design shows primarily astigmatism with a separation of the astigmatic foci of 0.3mm in the focal plane. The two focal curves shown in the figure are seen to have different focal points showing some residual astigmatism in the corrected wavefront as expected. The blue, horizontal line in the figure represents the expected 0.3mm separation. The design astigmatic separation is seen to be of about the size determined from the focal sweep curves, however a value up to twice as large would also probably be consistent with this data.

2) PSF properties:

Data Analysis

Figure 2 shows summary plots of the analysis of the total combined deep psf image composed of all 102 of the 103 individual exposures following dark subtraction. The flat field file flat_092799.fits has been applied to the image. The lower left panel shows a log stretched, 70x70 pixel region near the image core. The core is relatively narrow and the "ring" of light present in a halo at about 10-15 pixels from center is evident. The halo is not perfectly continuous but has brighter and fainter areas. The lower right and middle left panels show single pixel wide cuts across the PSF image in the vertical and horizontal directions respectively. The presence of the halo is most evident in the vertical profile; presumably the horizontal profile cuts between bright spots in the halo.

The MTF, determined from the image, is shown in the right, center panel in vertical and horizontal cuts. The MTF was calculated as the absolute value of the amplitude of the Fourier transform of the PSF image. The spatial frequencies have been normalized to the critical frequency for an *f/16.*6 system, $1/\lambda f$ (=0.095 cycles/micron = .857 cycles/pixel for the 9 micron, CCD pixels). For comparison, the diffraction limited MTF is displayed as a dashed line and the combination of a diffraction limited optical system and square pixel detector model displayed as a dotted curve. The detector model transfer function used was that detailed in Schroeder (1987), namely

$$T_a(\nu) = \exp[-0.282(\pi \nu a)^2]$$

Where a is the pixel width and ν is the spatial frequency. The diffraction limited MTF was generated from within a Zemax model of the DCATT system which includes the small residual astigmatism in the system design (a small effect on the MTF) and more significantly, the effect of the non-uniform pupil illumination. This was modeled using the Zemax pupil apodizing feature which is expressed as

$$A(\rho) = \exp[-G\rho^2]$$

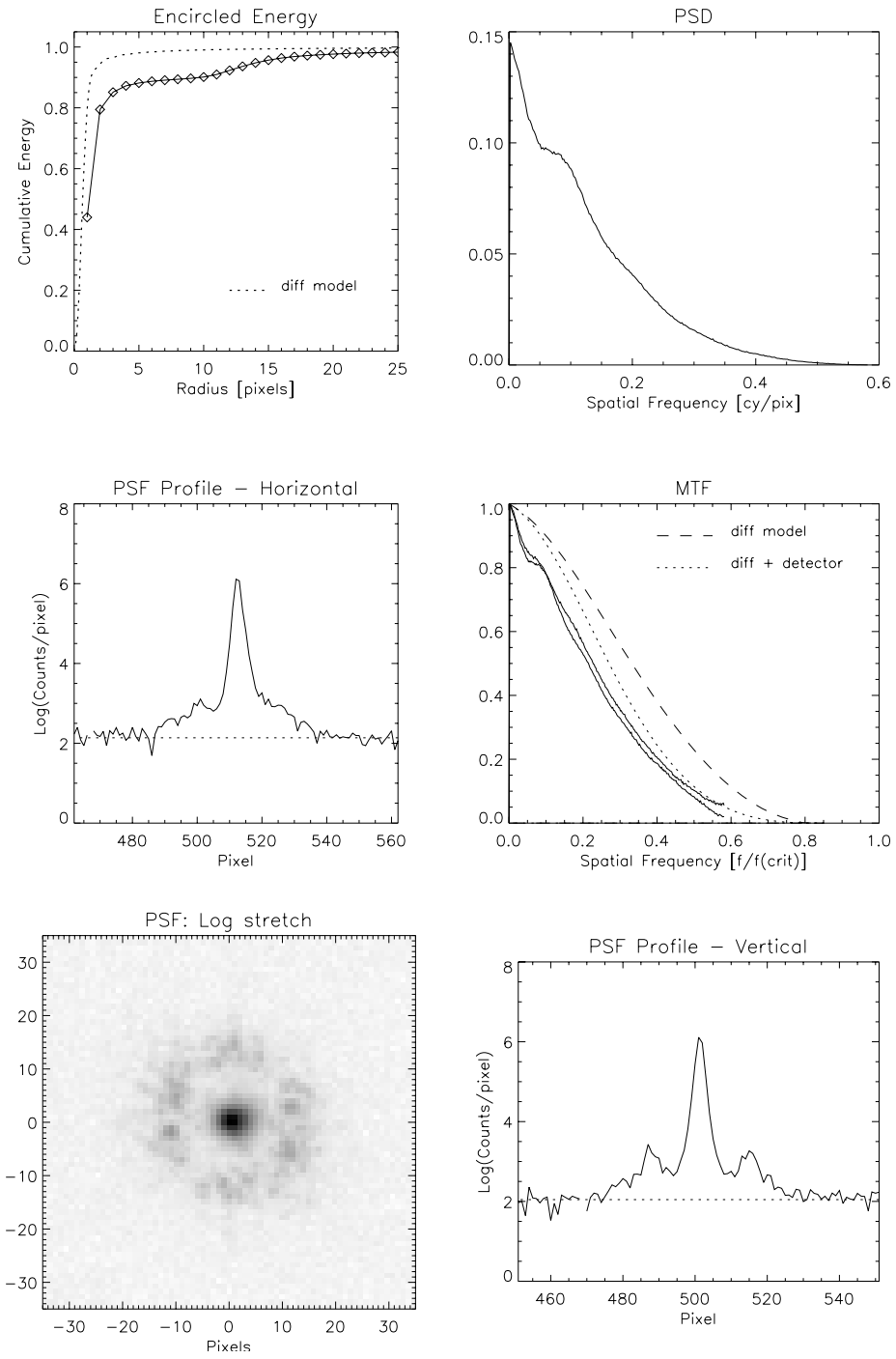

Figure 2: Summary plots of the analysis of the total, combined image from 29-Sep-99. Individual plots are (left to right,bottom to top): (a) a log stretched image of the PSF over a 70x70 pixel area, (b) a one column slice through the psf showing the vertical profile, (c) a similar one row slice showing the horizontal profile, (d) the MTF determined from the image in the vertical and horizontal directions with the optical only MTF (diff. Model) and the combined optical and detector model MTF, (e) the image encircled energy as a function of radius compared with the optical model (diff model), and (f) the power spectral density.

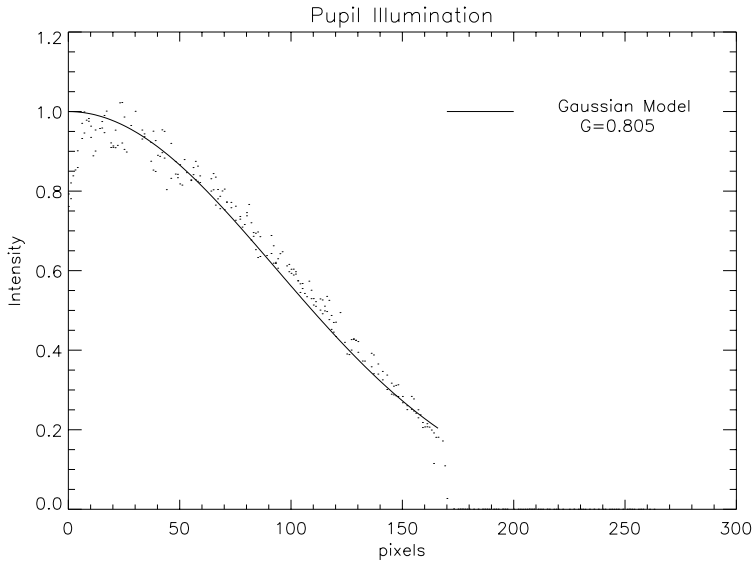

Figure 3: The pupil illumination is compared with a Gaussian model. Dots show the profile of the pupil illumination obtained using the pupil imaging lens during this test. The comparison model profile uses a G parameter of 0.805 and produces a good fit to the measured profile.

$A(\rho)$ is the field amplitude at the normalized radius ρ; the parameter G, sets the scale of the Gaussian amplitude. Intensity at the pupil is A^2. A profile of the exit pupil illumination as obtained during this test using the pupil imaging lens, is compared with a Gaussian intensity profile with G=0.805 in figure 3.

Not included in the MTF model is the effect of the source extent of the experiment. The source consists of an illuminated 5micron pinhole which is re-imaged onto a second 25 micron pinhole. The effect of this extended source will be a further, small decrease in the overall modeled MTF bringing it into closer agreement with the experimentally derived curve shown in Figure 2.

The general agreement between the model and measured MTF is reasonable at image spatial frequencies beyond about 0.09 with the main difference being a clear deficit in the measured values at image spatial frequencies below this point. An image spatial frequency of 0.09 is equal to 11 cycles/diameter in the pupil, where the DM is located. This pupil spatial frequency is just the ~Nyquist frequency of actuator control of the DM; the fixed actuator spacing prohibits WF control at higher pupil spatial frequencies resulting in the measured MTF deficit at lower image spatial frequencies. The DM allows correction of the high image spatial frequencies (close to the ideal value of the model) and subsequently high resolution using the usual criteria, however it does this at the expense of decreased modulation at low image spatial frequencies.

The result in the image plane of this reduced image MTF at low spatial frequencies is illustrated in the encircled energy plot shown in the upper left panel of Figure 2. The residual, highly correlated, WFE from the pattern of closely spaced DM actuators “scatters” light out of the core into the halo which is seen in the PSF image. Our measurements show about 85% of the light is contained within a radius of 3 pixels, 90% within a radius of 10 pixels, and then, encountering the halo, the EE increases by about 7% to a radius of 17 pixels. The remaining 3% of the light is at a radius >17 pixels. Also illustrated in the figure is a model of the expected encircled energy using a model of the ~Gaussian, non-uniform pupil illumination. Such a pupil illumination pattern actually apodizes the pupil reducing the illumination beyond the first diffraction zero and increases the encircled energy beyond this point when compared to the usual Airy diffraction pattern.

The PSD is shown in the upper right panel. The PSD was calculated as the squared amplitude of the Fourier transform of the PSF in vertical and horizontal slices.

In this experiment, the PSF core was under sampled; the Airy disk size fwhm is about λF = 10.5 microns compared to the 9 micron detector pixels. However, we can verify that the measured core width is approximately as expected. Fitting of the profiles of several of the individual images (to eliminate drift effects - see section 3) gave Gaussian equivalent fwhm of 1.8 - 1.9 pixels. Adding in quadrature the main components of image width as below gives:

Source	Magnitude [microns]	Note
~Airy disk fwhm	10.5	No wfe included - small effect
Detector pixel width	9	
~min source width	5	True width likely somewhat larger due to illumination system
~Individual frame jitter	1.5	
Total estimated fwhm	14.8	=1.64 pixels

Thus we get an estimate of expected fwhm of about 1.64 pixels compared to the slightly larger measured Gaussian equivalent width of 1.8 -1.9 pixels. Rearrangement of the illumination system will be made to ensure a true 5 microns source extent and future experiments will be made which magnify and provide higher sampling of the image core for more accurate comparisons.

Grating Analogy

An upper limit estimate of the energy contained in the well defined halo can be obtained by considering the residual phase variations detected in the pupil following DM correction, as a phase grating. This estimate should be an upper limit as it assumes the pupil phase errors are of equal magnitude and totally correlated. Since this is not the case (see the phase map shown in figure xx) such an estimate is mostly useful as an order of magnitude estimate and for guidance in scaling.

The first order efficiency for a sinusoidal grating should provide a reasonable model description of a periodic phase error in the pupil. From Loewen et al the first order grating efficiency for such a grating is given by

$$\varepsilon_{-1} = | J_1(w) |^2$$

$$w = \frac{2\pi}{\lambda} h$$

$$h = groove\ depth$$

$$\lambda = wavelength$$

$$J_1 = first\ order\ Besel\ J$$

Figure 4 shows a family of such efficiency curves over the range of 500 - 2000nm. Each curve is labeled by the rms WFE at 633nm, and the results at 633 and 925nm (two DCATT filters central wavelengths) are indicated by vertical lines.

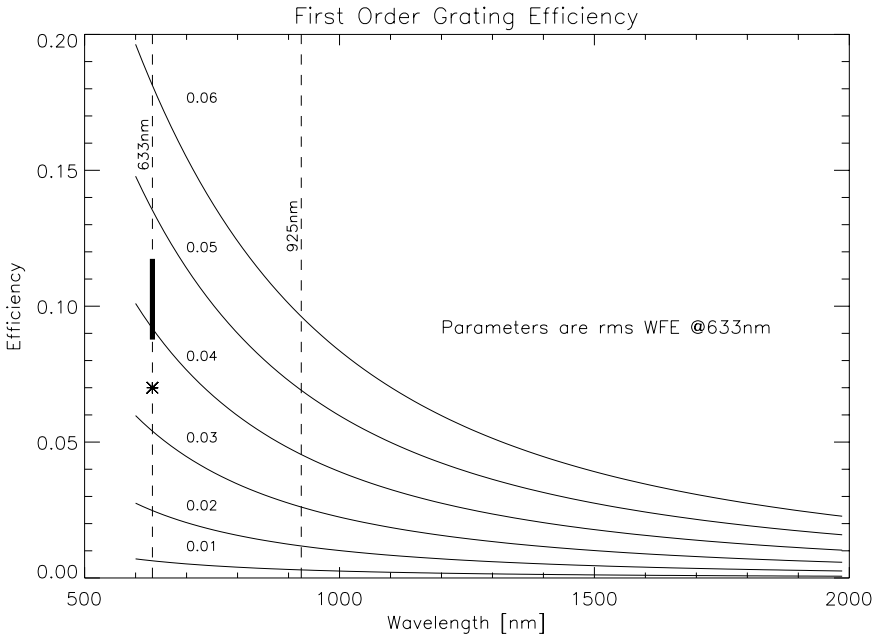

Figure 4: First order efficiency for a sinusoidal phase grating. The parameter label on each curve is the rms WFE @633nm. Vertical bars are placed at 633 and 925nm. The thick vertical bar at 633nm shows the range of WFE as determined from phase retrieval during the day of testing. The star shows the measured ~7% energy in the halo at 633nm.

The thick vertical bar at 633nm indicates the range of rms WFE determined throughout the test from the phase retrieval results. If the model was strictly correct, we might have expected 9-12% of the total light in the halo. The star, shows the ~7% energy actually measured in the halo, less than, but comparable to, the simple model estimate. Several simplifications in the model probably account for these differences. The model assumes perfect correlation across the pupil with repeated, equal height, sinusoidal phase errors and the model assumes continuous grooves. Neither assumption is perfectly correct so the model provides an upper limit to performance. However the model indicates how the scattered energy may be expected to scale with wavelength and residual WFE.

The model results indicate that the change of scattered energy with wavelength for a fixed rms WFE for such periodic phase structures varies approximately as λ^{-2}. Thus for equal WFE as determined in these tests at 633nm, we expect the scattered light in the halo at 925nm to be about ½ (~3.5%) and the value at 2 microns to be less than 1%.

Observatory Performance

Use of a DM in an astronomical observatory such as NGST with performance similar to that measured here should result in a similar, sharp PSF core. However as the sources in such astronomical cases are usually broadband, the halo would have a more complicated structure than measured in this ~monochromatic test. The halo would have an inner radius edge determined by the low wavelength cutoff of the observatory throughput. A much more extended halo structure than seen in this test would then be present from longer wavelengths in the passband. The grating model suggests rapidly reduced halo scatter with increasing wavelength which though may be counterbalanced by increasing observatory throughput as it's prime wavelength region is approached.

PSF stability throughout the observatory lifetime is also an important consideration. The rapid rise in halo scattering with correlated WFE (see Figure XX) suggests that small changes in the DM adjustment can result in a variable PSF structure, particularly in the details of light scattered into the resulting halo. As the DM will likely be used to "tune up" performance periodically during the observatory lifetime, the degree to which the same DM settings can be achieved will be an important factor in determining the detailed stability of the PSF structure.

Finally, it is clear how the performance demonstrated here can be improved. Increasing the number of actuators over the pupil (decreasing their spacing) will only have the effect of shifting the MTF deficit to lower image spatial frequencies, not removing it. With the same WFE as determined here, a higher actuator number DM will just shift the same amount of scattered energy farther from the core - it will not reduce the value. To reduce the amount of scattered energy, better control (lower amplitude of the residual WFE) will rapidly improve performance.

3) PSF prediction from Phase Retrieved Wavefront

Figure 5 (lower panels) shows a simulated PSF, in both linear and log stretch, generated from a WF estimate taken during the deep PSF exposure sequence. The simulated PSF is based on a pupil complex amplitude generated using the square root of the pupil image for the amplitude and the WF estimate for the phase. This synthetic pupil is propagated to the image plane by a Fourier transform and rebinned to the detector format.

The synthetic PSF shows the main features of the deep PSF: a sharp core, approximately square dark hole, and a halo of scattered light surrounding all. The core is sharper than that observed in the deep PSF, however. There are several possible reasons for this, with the most significant likely being:

- Resolved source. The source pinhole is 20 um in diameter, and is within the resolution limit of the AO optics.
- Jitter and image drift. The deep exposure centroid shifted during the exposure sequence, as discussed above. Additionally, high-frequency jitter will have a blurring effect.
- Defocus. Some small defocus may have been present

Several other effects may also contribute to broadening the core though likely at a less significant level including,

- Detector charge bleeding. Photons hitting a particular pixel on occasion generate electrons in adjacent pixels.
- focal ratio mismatch. A problem if the *f/* assumed in the phase retrieval differs significantly from the actual *f/*.
- Pupil intensity. These retrievals were done with a model that does not include the slight ellipticity of the pupil.
- Data scaling.

A better match to the deep PSF is obtained if the synthetic PSF is deliberately blurred. Figure 6 shows several different synthetic PSFs, with various combinations of defocus and convolution blurring compared with the actual deep image (upper left panel). All images are presented with a log stretch. The blur kernels are Gaussian, with half-widths as indicated in the plots. Reasonable comparisons are achieved for both the core and the halo with blurs of 0.4 - 0.8 pixels. This is consistent with the illumination source width (≥ 5 microns) and the jitter and drift (~0.4 microns), as the pixels are 9 um wide.

PSF from retrieved WF propagated to focal plane

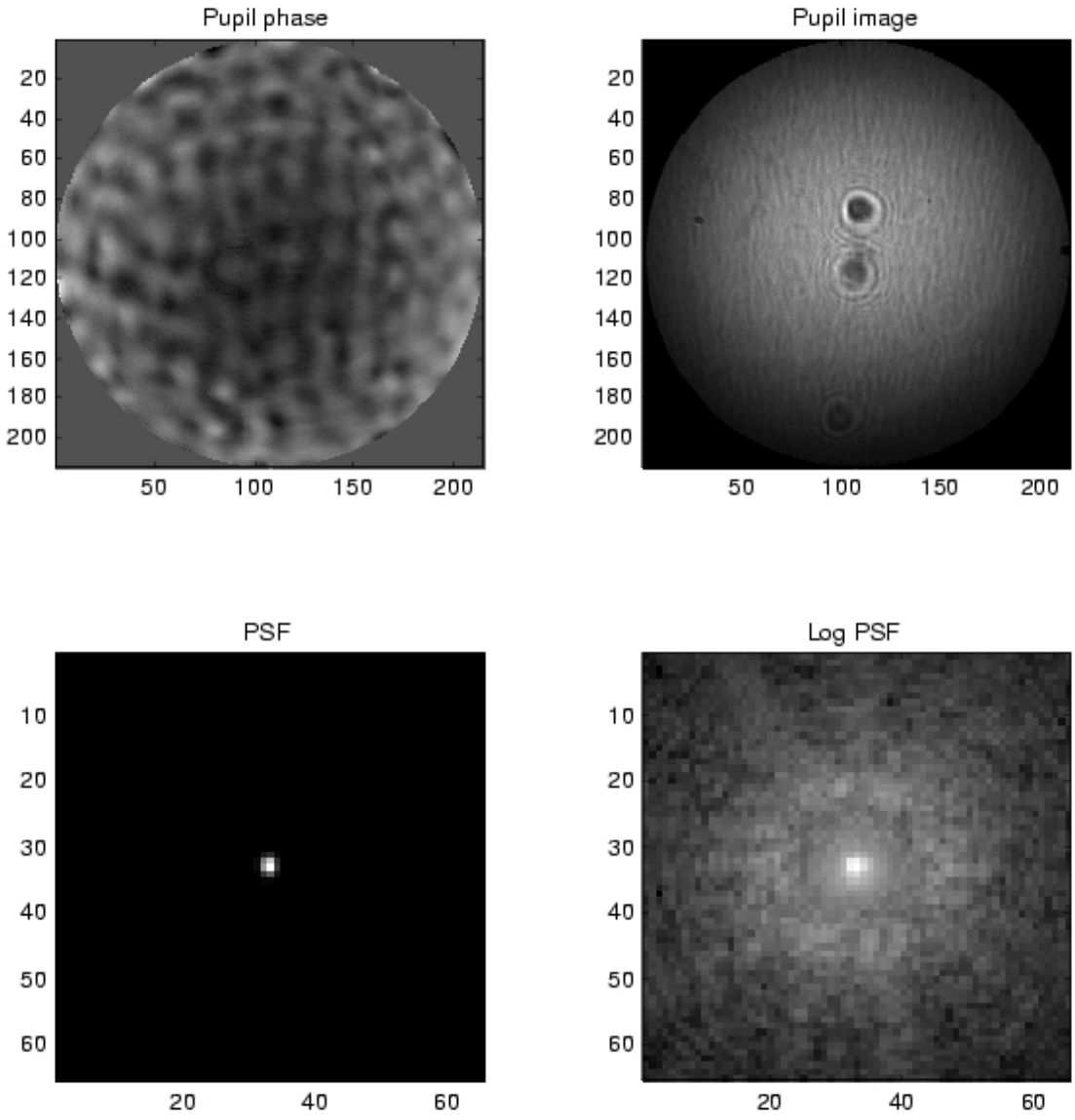

The retrieved **WF** estimate was used to generate a simulated in-focus image, for comparison with the deep **PSF**. The complex amplitude at the exit pupil was synthesized by using the square root of the pupil image data to define amplitude and the retrieved phase to provide the phase. The resulting complex amplitude matrix was propagated forward to the focal plane, and the image computed as the modulus squared.

Figure 5

Integrated PSF compared to projected PSFs

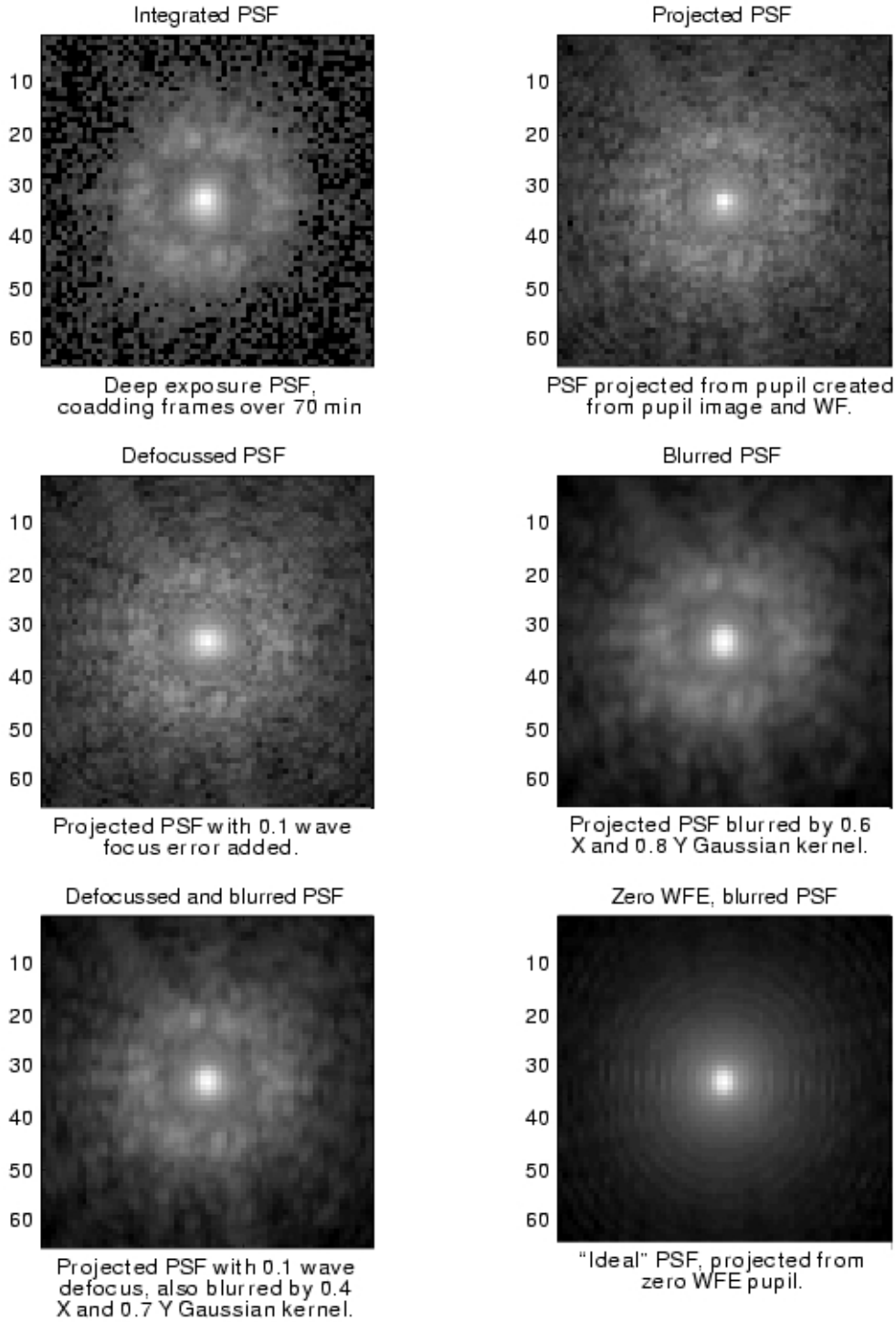

Figure 6

Ideal PSF (zero WFE, same pupil)

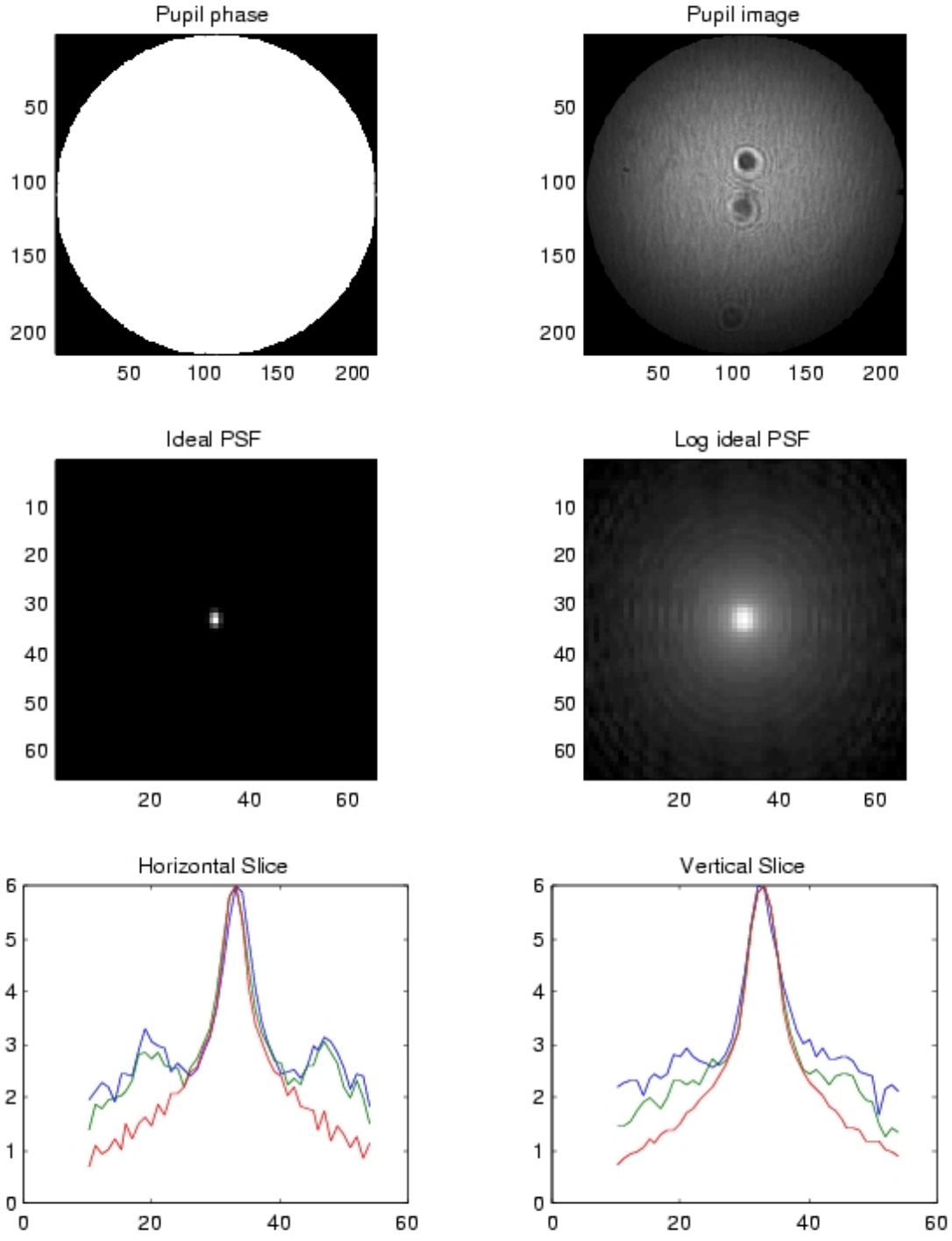

Slices show measured (blue), projected (green) and ideal **PSF** cross-sections, blurred by **0**.6 pixels **X** and **0**.8 pixels **Y** radius **G**aussian kernel.

Figure 7:

Measured PSFs taken at 2 different times

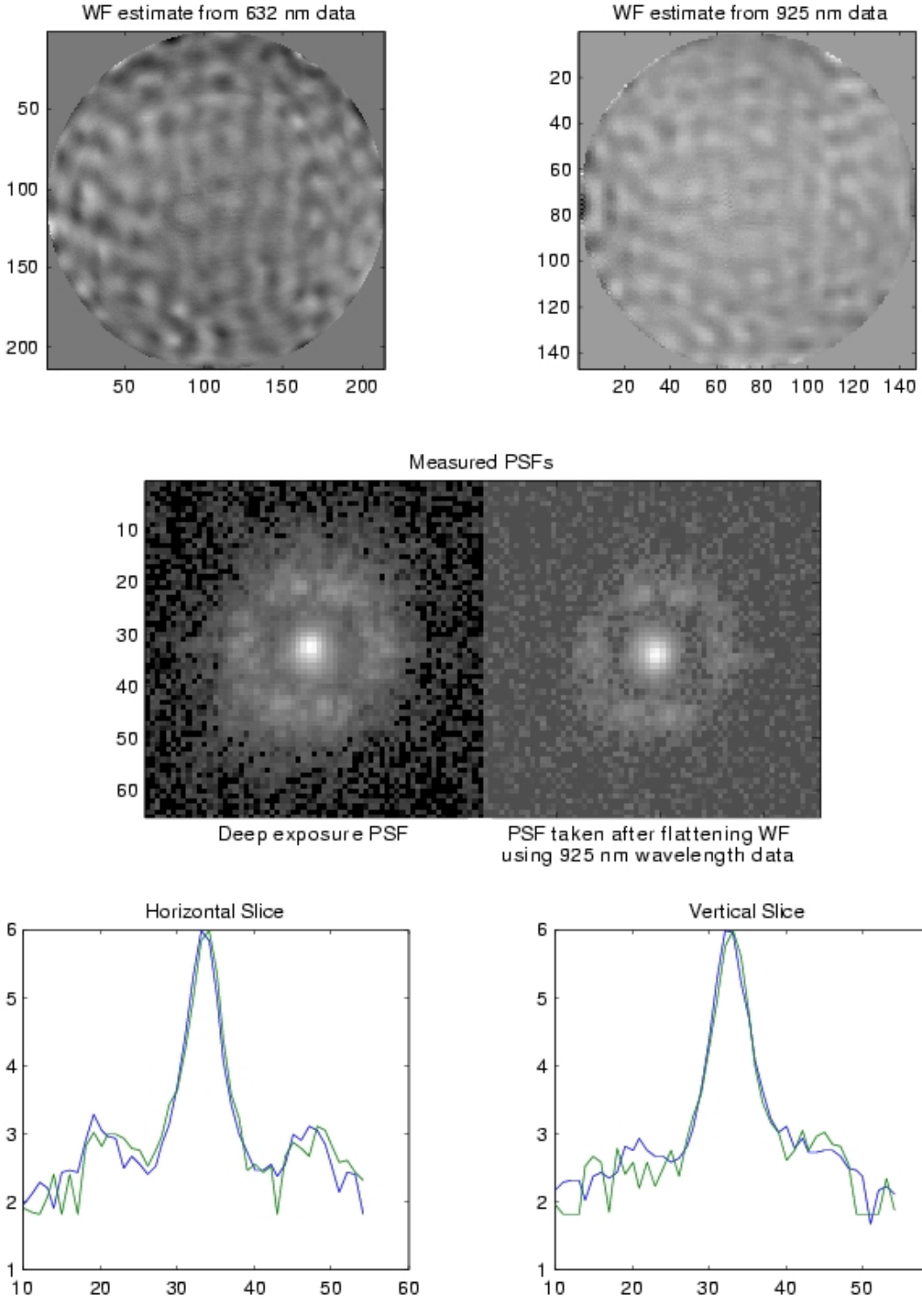

Figure 8:

Experience and analysis has shown that blurring effects are well tolerated by the phase retrieval WF sensing algorithm, provided the phase retrieval images are taken well out of focus. The main effect is to soften some of the hard edges that may be present in the pupil, such as segment boundaries.

The question of how good the PSF could be, given perfect control, is addressed in Fig. 7 , which shows an idealized synthetic PSF generated from a perfectly flat wavefront but using the measured non-uniform pupil illumination. The result, illustrated by PSF profiles in the lower two panels, is a core that very closely matches the data and blurred synthetic PSFs, but without the halo of scattered light. This result confirms the origin of the halo as DM control residuals.

Finally, Fig. 8 compares the deep PSF to a second PSF taken 3 weeks later (10/25/99), after the DM was reflattened using phase retrieval images taken at 925 nm wavelength. This was done to see if some wavelength-dependent effect might be degrading WF sensing performance. The longer wavelength is better sampled by the WF sensor camera, and the source is not as well resolved. The results show essentially no difference between the two PSFs, to the much higher noise level of the second PSF.

4) Image stability (drift, psf variation, attempts to re-sample)

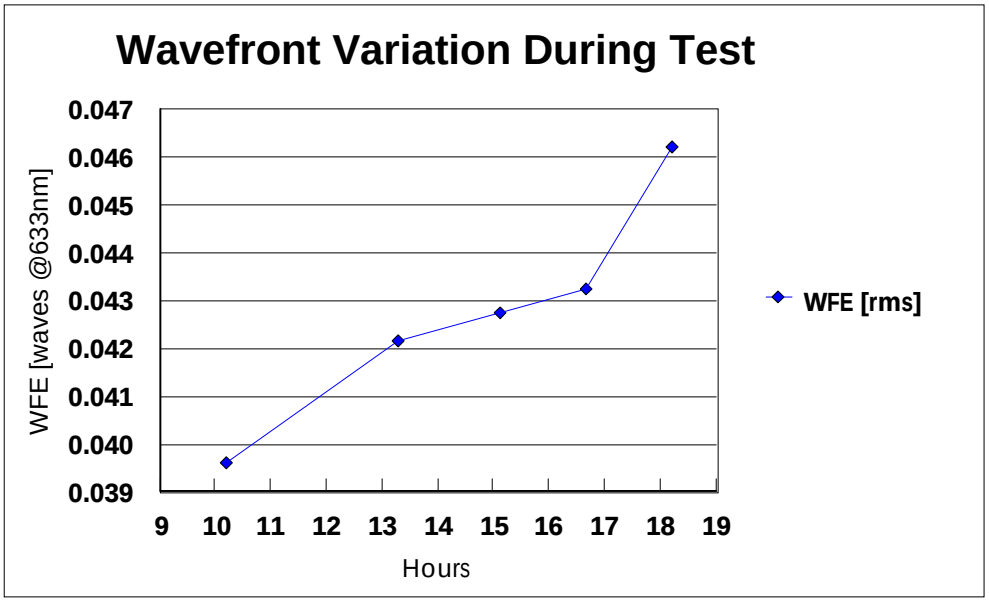

Figure 9 increase with time suggests a systematic degradation of the wavefront and not just the expected wavefront sensing process noise.

The long time of this experiment and the large number of images acquired allows a more systematic look at the environmental stability of DCATT over an extended period than has been previously performed. The summary data of this analysis in presented in Figures 9 and 10.

Figure 9 shows the rms WFE as determined from the repeated phase retrieval procedures conducted during the day. There is expected to be some degree of random error in the wavefront sensing process; earlier tests at JPL with similar experimental conditions on another deformable mirror showed average rms differences from a nominal flat condition of $\lambda_{633}/115 = 0.009\ \lambda_{633}$. The data in Figure 9 is formally consistent with this

result. However, the monotonic degradation suggests that there may be some systematic instability in the wavefront and not just random variation due to the sensing algorithm. Examination of the phase retrieval results may allow a clear distinction to be made between random variations in the WF or "smooth" variation of WFE with time (defocus, for example).

Figure 10, shows various analyses of the position of the image centroids of each of 80 images obtained over a period of about 70minutes. There is clear indicating of image drift of about 0.4 pixels in X and 0.2 pixels in Y over this time period. While this value is small, it undoubtedly contributes somewhat to the broadened PSF core. A jitter value of about 0.15 pixels rms is also indicated from the spread of the centroid values about the mean drift. This is consistent with earlier jitter tests showing 0.1 - 0.2 pixels jitter over short time periods. As the CCD shutter time is limited to $\geq$ 0.1s, any higher frequency jitter will not be determined from such data.

Further Work:

1) Repeat for core using magnifying lens
2) Repeat at other wavelengths to determine the scaling of the halo with wavelength. Also do a broadband image.
3) Look at stability of the dark frames.
4) Check variability of psf with small changes in DM & WFE.
5) Determine if apparent WFE increase with time is due to smooth wf changes (ex. Defocus) or to actuator relaxation.

References

1. Schroeder, D. J., "Astronomical Optics", 1987, p 312.
2. Loewen, E.G. , Neviere, M. And Maystre, D. , JOSA, 68, 496.

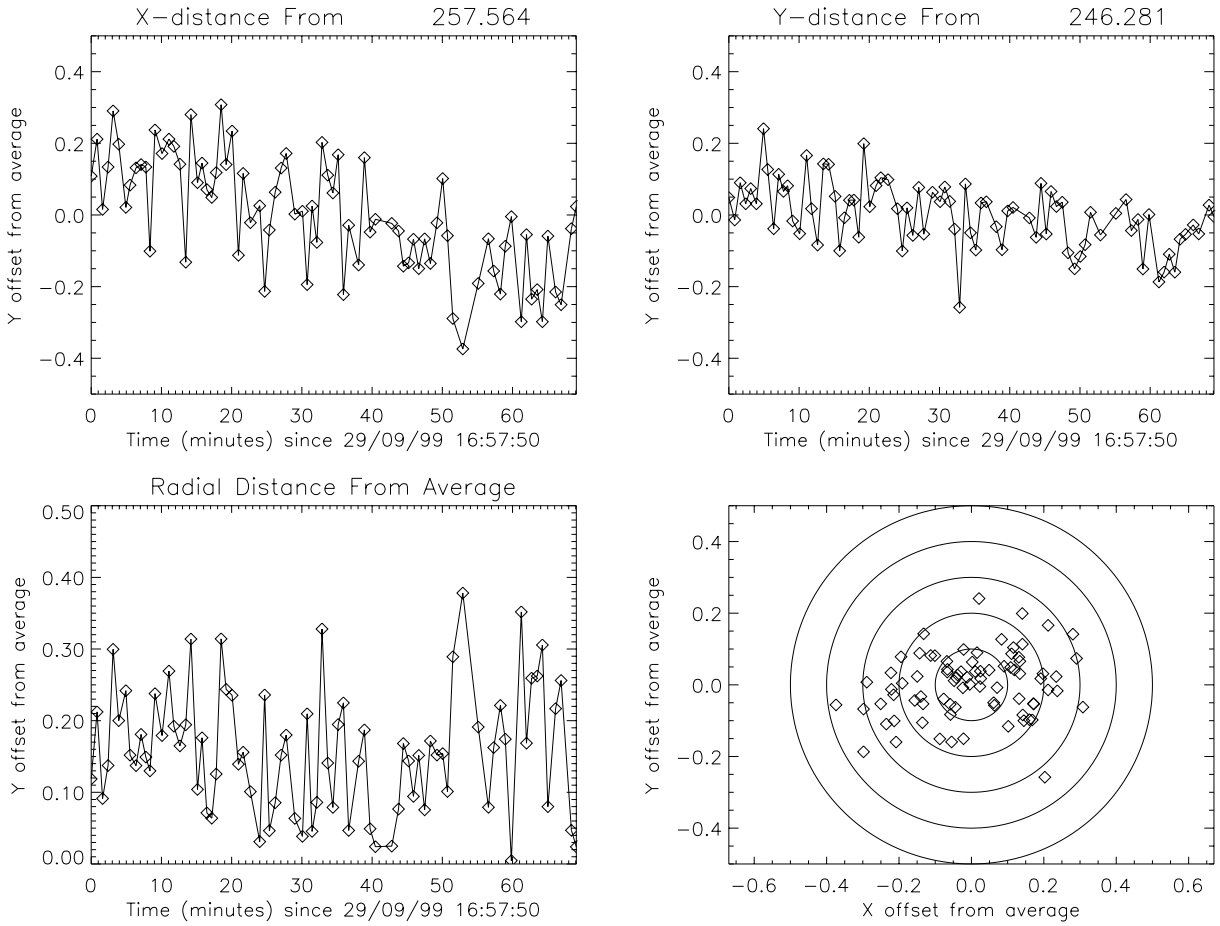

Figure10: A series of plots showing the image drift over about 70 minutes as determined from the motion of the image centroids. The plots show (left to right, top to bottom) (a) the offset in pixels in the detector Y direction (vertical) , (b) the image horizontal (X) drift, (c) the radial drift from the average centroid position, and (d) a plot showing the XY distribution of the image centroids. The image drifted about 0.4 pixels in X and about 0.2 pixels in Y during the 70 minutes.